IEEE Access
Multidisciplinary ⋮ Rapid Review ⋮ Open Access Journal

Received 10 August 2022, accepted 14 August 2022, date of publication 26 August 2022, date of current version 8 September 2022.

Digital Object Identifier 10.1109/ACCESS.2022.3202210

RESEARCH ARTICLE

High-Power Shape Memory Alloy Catapult Actuator for High-Speed and High-Force Applications

PHILIPP MOLITOR[1,2], ROUVEN BRITZ[2], AND PAUL MOTZKI[1,2]

[1]Intelligent Material Systems Laboratory, Center for Mechatronics and Automation Technology (ZeMA gGmbH), 66121 Saarbrücken, Germany
[2]Intelligent Material Systems Laboratory, Department of Systems Engineering, Department of Materials Science and Engineering, Saarland University, 66123 Saarbrücken, Germany

Corresponding author: Philipp Molitor (philipp.molitor@imsl.uni-saarland.de)

ABSTRACT Nickel-Titanium (NiTi) based shape memory alloy (SMA) wires are already often used in industrial actuator applications. Their high energy density allows the building of light-weight actuator systems with high forces using small installation spaces. Combined with the biocompatibility of NiTi, a huge field of applications can be covered by SMA actuated systems. In systems like emergency brakes or switch disconnectors, which require high forces as well as high actuation speed, the high-power capability of NiTi actuators is exploited. The presented work details the development and characterization of a giant power catapult demonstrator, that combines the high-speed and high-force capability of SMA wires. To illustrate the vast force, speed, and power potential of SMA wires, a bowling ball is launched from its resting position vertically into the air using SMA wires. For demonstration purposes, a target altitude for the bowling ball of 500 mm is chosen. With the height and the overall accelerated mass given, an actuation force $F \cong 920$ N is needed. The instantaneous energy release from the designed power source results in the targeted flight height and an overall peak power of $P \cong 0.5$ MW.

INDEX TERMS Keywords actuator, catapult, high-force, high-speed, high-power, high-performance, NiTi, Nitinol, shape memory alloy, SMA.

I. INTRODUCTION

Shape memory alloys (SMA) are well known for their superelasticity as well as their actuation capabilities and are widely used in biomedical applications and specific actuator products [1], [2], [3], [4]. The high energy density of Nickel-Titanium (NiTi) based SMAs [5], [6], [7] allows for the development of high force industrial actuator applications and robotic structures [8], [9], [10], [11], [12]. The notion Nitinol, as a common name for the alloy, is an acronym for the two given components and the place of its discovery. The discovery of the shape memory effect of a binary nickel and titanium alloy is attributed to William J. Buehler and Frederick Wang in 1959 over the course of their research at the Naval Ordnance Laboratory. The shape memory effect is based on the property of the alloy to perform a reversible phase transformation. One distinguishes between the monoclinic low-temperature phase martensite and the cubic space centered high-temperature phase austenite [13], [14]. In contrast to plastic deformation in conventional metals, which leads to a displacement of atoms within the crystal lattice, shape memory alloys show a phase shift in the martensite structure without a displacement of atoms. This so called pseudoplastic deformation is reversible and can be revoked [15], [16]. Heating the structure leads to a phase transformation towards austenite, which comes with a change in macroscopic shape. In the case of SMA wires, the temperature induced transformation to the austenite phase results in a contraction of the SMA wire, which is used to perform mechanical work in actuator systems [17].

Current research in the field of SMA actuators has a strong focus on identifying new areas of application like the field of bio-inspired motion [18], [19], soft robotics [20], [21] as well as modeling and control of the oftentimes complex nonlinear material behavior [22], [23].

Based on their performance capabilities, SMA actuator applications can be classified into fast responding systems

The associate editor coordinating the review of this manuscript and approving it for publication was F. R. Islam.

[24], [25], [26], [27], [28] and those that move very high loads [29], [30].

The content of this paper deals with combining both topics in a descriptive way, resulting in a mechatronic system for technology demonstration purposes. Dana, Vollach and Shilo give an overview of these high-rate SMA applications [27], which can be used for the development of quick release mechanisms in safety applications [26] or contactors as prominent practical examples. In both cases, the SMA actuator must provide high forces in the range of several micro- or milliseconds to either pull a safety pin and activate a brake-/blocking mechanism or disconnect/break a high-voltage and high-current electrical circuit.

To demonstrate both, the possible velocity and the potential force in a complete mechatronic technology demonstrator system outside a laboratory, this work aims to accelerate a bowling ball vertically into the air from rest using only SMA wires. To sufficiently demonstrate this dual high-performance effect, a certain flight height of the bowling ball is necessary. This flight height consequently determines the energy required to accelerate the ball, so that it reaches the desired height.

After defining the design and in consideration of the necessary mechanical and electrical parameters, a demonstrator is designed, built, and put into operation.

The remainder of this paper is composed as follows. In section II, an overview of the overall system concept is provided and the mechanical and electronics designs are presented and discussed. Furthermore, the applied SMA wire bundle configuration is introduced and validated. The final demonstrator setup is described in section III, as well as the possible performance of the developed system. Decisively, an outlook is given and concluding thoughts are discussed in section IV.

II. ACTUATOR SYSTEM CONCEPT, DESIGN, AND VALIDATION

The purpose of the presented demonstrator is illustrating the immense power potential of SMA wires respectively the SMA technology. To accomplish that goal, the actuator system is divided into two main systems, i.e., the mechanical guidance framework and the electronical power- and switching system. As mechanical conditions, a desired flight altitude of $h = 500$ mm and an overall mass m to be accelerated of approx. 3 kg are chosen. The needed kinematic momentum for the acceleration of the mass of the moving system is generated from the contraction of the SMA wires whilst their phase transformation from martensite to austenite using an electrical current. During this thermally induced transformation of the crystal lattice, a corresponding strain of 4% of the material is achieved. Regarding the parameters for height, mass and short acceleration travel, a force of $F \cong 920$ N is needed. Due to the high forces, SMA wires with a diameter of $d = 500$ μm are chosen and put in a radial formation of 3 bundles [31] with 4 wires each. To store the necessary electrical activation energy, a circuit board is designed with an array of capacitors and a maximum operation voltage of 450 V. With the chosen high-power switching components, a current flow of over 600 A per bundle and thus a combined system current flow of over 1800 A can be achieved. This high current through each bundle results in an almost immediate transformation of the crystal lattice from martensite to austenite and the corresponding contraction of the SMA wires.

To gain the maximum effect of the demonstrator, a concept was elaborated combining both parts in an efficacious fully integrated mechatronic system.

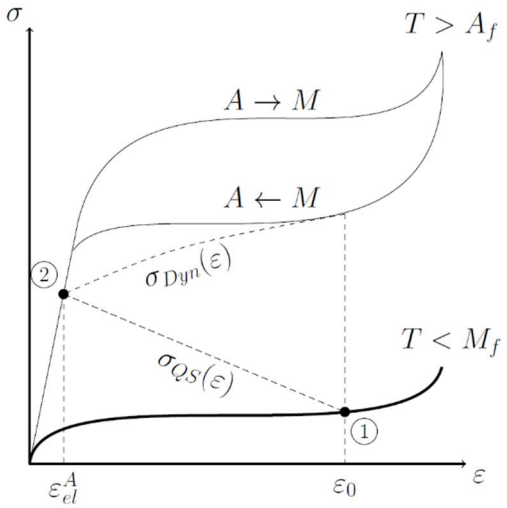

FIGURE 1. Mechanical stress-strain behavior of SMA wires in low temperature (martensitic) and high temperature (austenitic) states [27].

A. BASIC CALCULATIONS FOR DESIGN

As concept base, all needed kinematic parameters have to be evaluated and set. The activation scheme in this demonstrator aims at full SMA wire contraction with maximum velocity and thus generating an acceleration of a mass. Even though the mechanical stress-strain behavior of SMA wires is highly non-linear and hysteretic (Figure 1, [27]), in this specific case the only constraint is to reach the fully austenitic branch (2) from resting position (1) as fast as possible. This means, no further control of the actuator is needed or intended, the only goal is maximum power release upon activation.

Based on energy conservation, with gravity g and the required height of $h_1 = 500$ mm, the necessary velocity v_1 of the launched bowling ball can be calculated as:

$$v_1 = \sqrt{2\,g\,h_1} = 3.13\,\frac{\mathrm{m}}{\mathrm{s}} \tag{1}$$

Furthermore, with the chosen SMA wire length of $l_{martensite} = 400$ mm, the presumed strain of 4% and the resulting wire-length-based acceleration travel of $\Delta x = 16\ mm$, the remaining translatory motion parameters, acceleration time t_1 and the corresponding acceleration a_1,

can be evaluated:

$$t_1 = \frac{2\Delta x}{v_1} = 10.22 \text{ ms} \tag{2}$$

$$a_1 = \frac{v_1}{t_1} = 306.26 \frac{\text{m}}{\text{s}^2} \tag{3}$$

The correlative combined force F can be calculated, considering the kinematic mass $m = 3kg$ and the needed acceleration a_1 from formula (3), as:

$$F = m\, a_1 \cong 920 \text{ N} \tag{4}$$

In perspective of these high forces, SMA wires with a diameter of $d = 500\ \mu$m were picked and put in a 3 by 4 wire radial bundle arrangement (Figure 2).

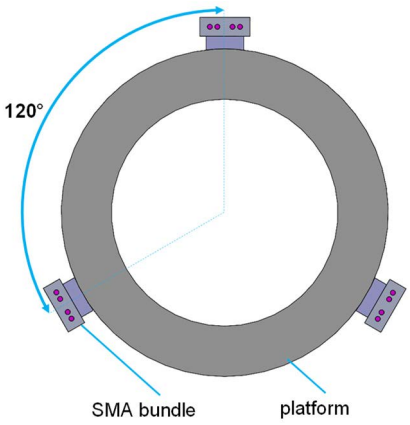

FIGURE 2. Drawing of the radial SMA bundle arrangement used for the bowling ball catapult.

With Equation 4 and the relevant values of the mass of a single wire $m_{SMA} = 0.53$ g, the specific thermal capacity $c = 500$ J/kg K, the specific enthalpy $h = 20$ J/g and the phase transformation temperature rise $\Delta T = 73$ K, the required activation energy W_1 per 4-wire bundle can be calculated.

$$W_1 = 4W_{1,1} = 4m_{SMA}(c\Delta T + h) = 119.12 \text{ J} \tag{5}$$

To deploy the calculated energy in the given time t_1, a dedicated energy source combined with capable control and switching electronics is necessary.

B. MECHANICAL DESIGN

As the SMA wires are exclusively responsible for the demonstrator kinematics, a proper mechanical design is developed to illustrate this matter.

To provide the needed force and power, special SMA wire bundles are designed. The bundle brackets can hold up to 5 wires each. At the moment of launch, every individual SMA wire is providing a maximum peak force of 76.5 N with a corresponding maximum peak mechanical stress of 390 MPa. The wires are set in parallel mechanically and electrically, whereas the clamping stem is also serving as the electrical contact for the SMA wires (Figure 3a). A more detailed view of the clamping bracket is shown in Figure 3b.

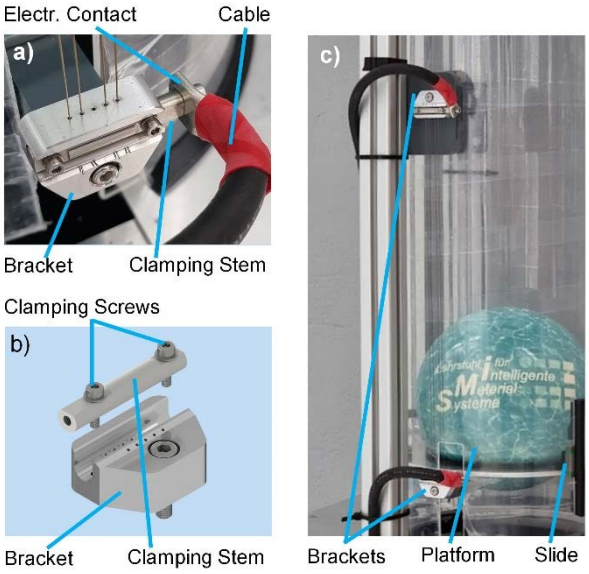

FIGURE 3. a) SMA bundle (bottom bracket) with 2AWG wire attached to the clamping bolt, b) image of the CAD design of the clamping bracket, c) corresponding SMA bundle attachment at top (frame) and bottom (catapult platform).

For the fabrication and assembly of the used SMA bundles, a specific preconditioning routine including a defined biasing mechanism is used, which ensures homogeneous elongation and stress level of $\sigma_1 = 250$ MPa of each wire in a bundle. This guarantees that all SMA wires have the same preconditions before their installation and minimizes individual residual strains.

The bowling ball is set on a brim of aluminum, operating as a catapult platform. One side of the SMA bundles is attached to this brim in a circular arrangement of 120° spacing. Additionally, the platform is mechanically connected to slides guided on linear rails. These rails are connected to a transparent acrylic tube, which has the task of keeping the linear rails in position and guiding the bowling ball on its flight trajectory. To limit the maximum travel of the catapult platform to 16 mm, which is the maximum SMA wire contraction and thus the highest possible acceleration path length, limit stops are attached to the linear rails. This prevents the platform from overshooting and ensures safe separation of the bowling ball from the platform after the acceleration travel, to allow the bowling ball to lift off. The selected position of the end stops was determined, and no variation was made, as the highest possible performance (flight altitude) was aimed for. Therefore, the longest possible acceleration path, i.e., the highest possible active stroke of the SMA bundles used, determines the position of the end stops. A reduction or increase would have no or a negative effect on the performance. For overall sturdiness, the mentioned arrangement is put in a frame of extruded aluminum profiles. The framework is divided into two chambers, the upper one housing the kinematics and the lower the control and power electronics. The other side of the SMA bundles is attached to the upper area of the aluminum frame (Figure 3c).

The platform with the resting bowling ball (Figure 4) is accelerated, as the 3 SMA bundles are activated. As the platform hits the limit stops (Figure 4, dashed lines), the bowling ball leaves the platform, continuing the vertical translatory movement until reaching the turning point at the targeted height. The movement then inverts, leading to the bowling ball landing back on the launching platform. After re-lengthening the SMA wires, the process can be repeated.

The evaluation of the electronic parameters, as well as the design of the control and power electronics, is described in the following section C.

C. CONTROL AND POWER ELECTRONICS

To supply the needed energy in the time t_1 for the SMA wire transformation, a suitable current source is crucial. As commercially available power supply units are either too slow or too expensive, a custom power supply was designed. In Figure 5, a block diagram is shown, which illustrates the interconnection of the core components. For safety reasons, an array of electrolytical capacitors was picked as energy storage.

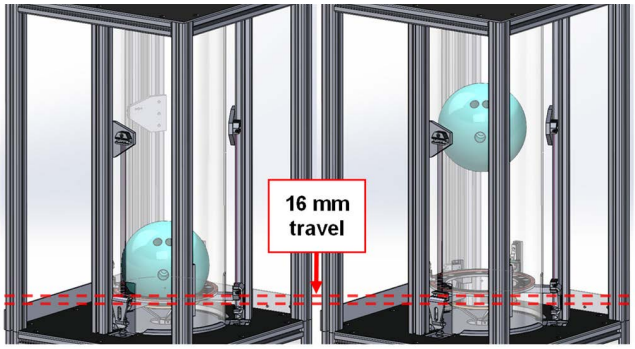

FIGURE 4. Illustration of the bowling ball in its starting position and when reaching the turning point after the lift-off subsequential of the 16 mm acceleration travel.

With an electrical resistance $R_B = 0.45\ \Omega$ per 4-wire SMA bundle, an assumed remaining charge of 0.7% of a discharged capacitor and being $\tau_1 = R_B \cdot C_B$, the relevant capacity can be calculated as:

$$U_C = U_1 e^{\frac{-t_1}{\tau_1}} = U_1 \cdot 0.007 \tag{6}$$

$$C_B = -\frac{t_1}{R_B\, ln\,(0.007)} = 4.6\ \text{mF} \tag{7}$$

Regarding the needed activation energy of $W_1 = 119,12$ J per bundle, the corresponding minimum charging voltage U_1 and the resulting electric current I_1 for a single bundle can be calculated:

$$U_1 = \sqrt{\frac{W_1}{0.5 C_B}} = 227.6\ \text{V} \tag{8}$$

$$I_1 = \frac{U_C}{R_B} = 505.8\ \text{A} \tag{9}$$

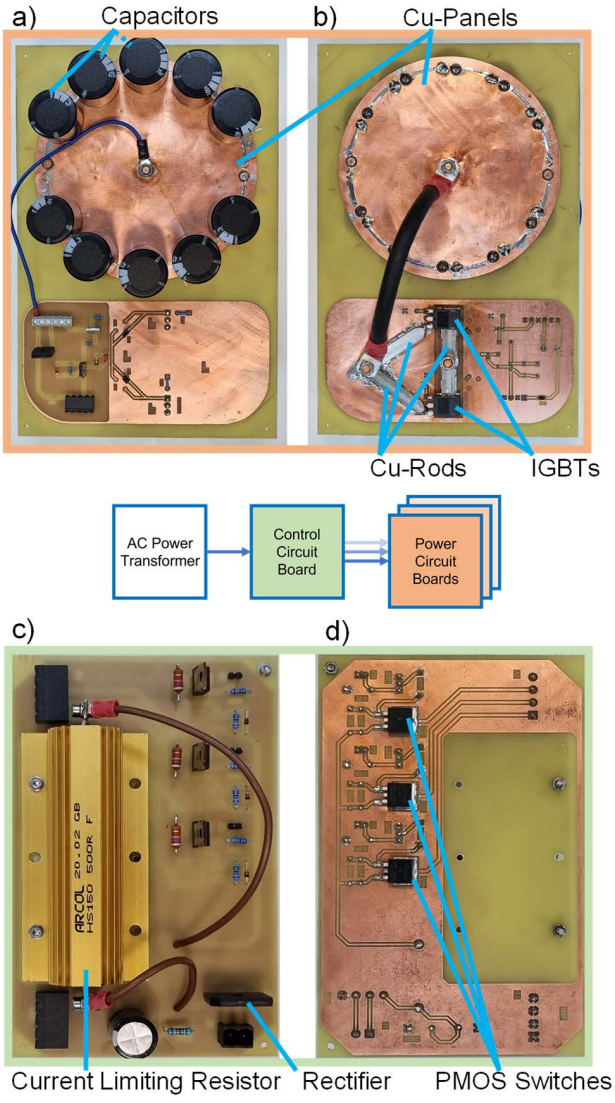

FIGURE 5. Block diagram of the charging circuit with a) power circuit board (top side), with 10/12 connected capacitors and secondary components, b) power circuit board (bottom side), with additionally applied copper sheets and rods leading the current flow from the capacitors through the IGBTs to the SMA wires c) control circuit board (top side), with limiting resistor, full-wave rectifier and secondary components, d) control circuit board (bottom side), with 3 high-power PMOS switches.

To provide the calculated capacity, the circuit board is designed to house up to twelve parallel connected 460 μF capacitors (Figure 5a), which allows an additional buffer of 20% to the needed ten capacitors.

As main switching component, two parallel connected insulated-gate bipolar transistors (IGBT) are used, which allow a maximum current flow of 960 A (Figure 5b). To enable a high-current flow, extra copper plates and rods were made and applied to the circuit board (Figure 5b). Additionally, the circuit board is equipped with all necessary state-of-the-art safety and regulation components like a blocking diode and discharge power resistor, to ensure the proper behavior.

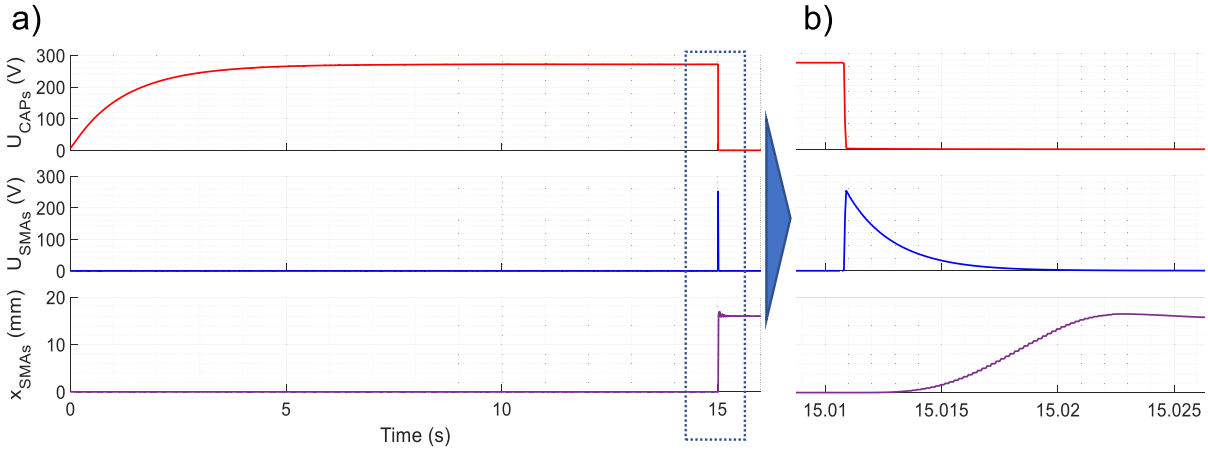

FIGURE 6. Illustration of the charging voltage of the capacitors (top), the voltage drop over the SMA wires (mid) and the resulting strain, respective travel of the SMA wires (bottom) as an a) exemplary sequence of events, b) detailed view at the moment of release.

For charging the capacitor array, the control circuit board is connected to an adjustable AC transformer combined with a full-wave rectifier (Figure 5c), which allows a charging voltage U_1 up to 350 VDC.

Each bundle is served by a dedicated capacitor-based power supply, which all are preconnected to the central control circuit board. On the control board, the charging and discharging of the capacitors is managed sequentially with 3 high-voltage p-channel MOSFETs (Figure 5d), combined with current limiting resistors (Figure 5c) for the charging process. The 3 power circuit boards as well as the control circuit board are connected to a microcontroller, which controls all the relevant sequences of the launching procedure.

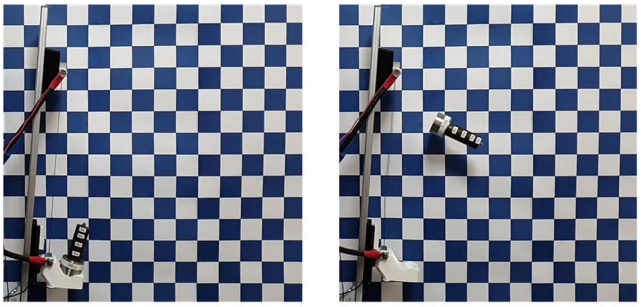

FIGURE 7. Display of the validation setup with relative overall accelerated mass in its starting position (left) and reaching its peak altitude (right).

D. SMA BUNDLE VALIDATION

To verify the functionality of the charging electronics as well as the capacitor based high-current power circuit boards, all parts are tested in a measurement setup linked to several sensors, e.g., *LEM HASS500* current sensor and a *Keyence LK-G87* laser triangulation sensor. To approach the full potential of the setup, the power circuit board is equipped in steps with 5, 8 and finally 10 capacitors. Corresponding to the number of capacitors, 2, 3 or 4 SMA wires are put in the bundles and activated by discharging the capacitors via the SMA wires.

During the charging and discharging process, the voltage of the capacitors, the voltage at the SMA wires, the current flow through the SMA wires, the contraction time, as well as the contraction travel are measured. Figure 6a shows the exemplary sequence of events from charging the capacitors until the instant of the momentary energy release, with the capacitor charging voltage at the top, the measured voltage at the SMA wires in the middle and the performed travel at the bottom. A more detailed view of this measurement is shown in Figure 6b. Additionally, a portion of the overall accelerated kinematic mass is put on a linear slide with a launch pad, attached to one side of the SMA bundle, in relation to the used count of SMA wires and capacitors. As the capacitors are discharged, the proportional weight is accelerated and launched equally to the bowling ball into midair (Figure 7). As the height of the launched weight reached is also measured, the charging voltage of the capacitors can be compared to the theoretical value of $U_1 = 230$ V and later adjusted to reach the aimed flight height. Regarding the measuring results of the validation process it is shown, that with the designed electronics an almost instantaneous discharge via the SMA wires is possible (Figure 8, center diagram) leading to the targeted 16 mm travel (Figure 8, bottom diagram). Furthermore, with an adjusted charging voltage of $U_2 = 280$ V (Figure 8, center diagram) all relative combinations of SMA wire and capacitor count and their corresponding weight the resulting performance can be measured. A maximum current flow of up to $I_2 = 560$ A (Figure 8, top diagram) can be monitored, leading to a discharge time of $t_2 \leq 11$ ms (Figure 8, bottom diagram). The travel exceeding the 16 mm mark, can be explained by the not completely stiff carrier, leading to the overshooting as shown in Figure 8. These experiments are repeated with every power circuit board, until all three needed circuit boards are validated and equipped with ten 460 μF capacitors, providing the needed capacity of 4.6 mF each.

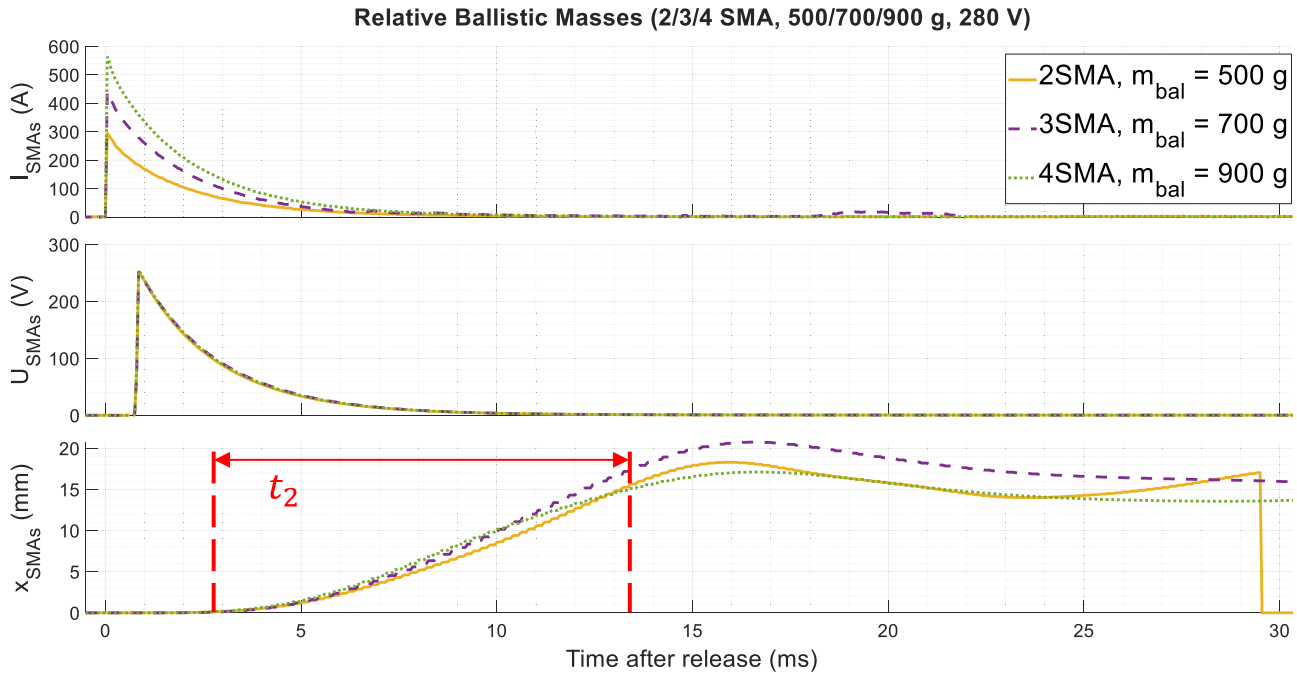

FIGURE 8. Representation of the current flow via the SMA wires (top), the voltage drop over the SMA wires (mid) and the resulting acceleration travel of the SMA wires (bottom) for the combined sequence of events with 2, 3 and 4 SMA wires attached with corresponding charging voltage and the proportional weight lifted. The red marker highlights the acceleration times $t2 \leq 11$ ms of each setup.

Subsequently, all electronics and mechanical components are assembled, combined, and put into operation, which is described in the following section III.

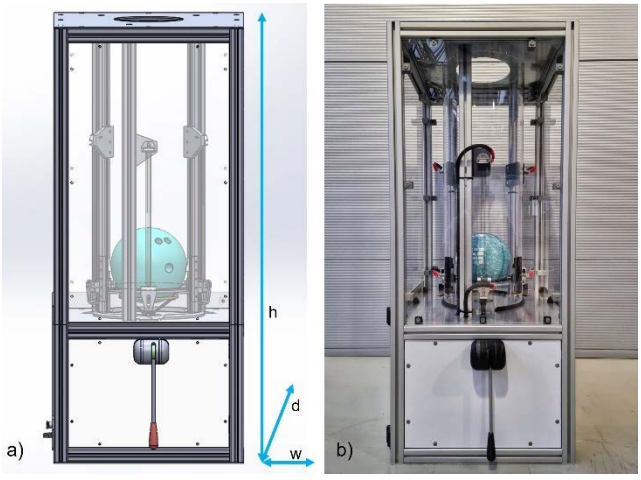

FIGURE 9. a) Image of the CAD assembly, b) Final fully assembled and enclosed demonstrator (height $h = 1260$ mm, width $w = 545$ mm, depth $d = 545$ mm) with top kinematic chamber and bottom electronics chamber.

III. FINAL SETUP AND PERFORMANCE

To examine the combined potential of the three power circuit boards and to compare the reached height of the bowling ball with the calculated height, all components are assembled. As mentioned above, the upper chamber of the aluminum framework serves as sturdy and reliable structure for the mechanical components (Figure 9). Apart from that, the bottom chamber contains all the electronics, such as the power circuit boards, the control circuit board, the microcontroller and necessary secondary components. The chambers are locked up with acrylic and aluminum composite panels (Figure 9) to ensure safe operation and handling. As the aimed current flow and voltage represent a high risk for human health, all the electronic connections are precisely built and thoroughly checked. Consequently, the whole setup is put into operation by applying stepwise rising charging voltages to the capacitors. The following discharge of the capacitors via the SMAs and the resulting movement is monitored and then compared to the expected behavior. Since the observed behavior matched the predictions, the charge voltage is incrementally increased until the target voltage of $U_2 = 280$ V.

The bowling ball is then placed on top of its launching platform and a square patterned sheet is applied at the back side of the demonstrator. Considering the square edge length of 5 cm, the travelled height of the bowling ball can be easily determined.

The first set of attempts is performed with a charging voltage of $U_2 = 280$ V, leading to a travel height of $h_2 = 41$ cm (Figure 10a, dotted red lines), a measured overall system activation energy $W_2 = 435$ J and a combined overall system power $P_2 = 0.43$ MW (Figure 10b). The sequence is repeated five times with always comparable results. Although the reached height presented itself very impressive, it minimally

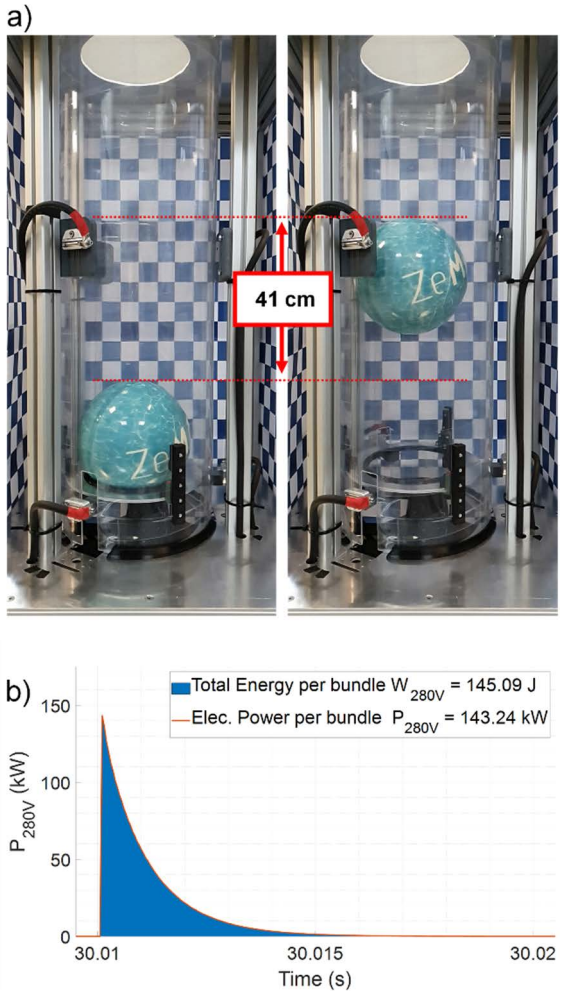

FIGURE 10. a) Comparison of start and end position (red dotted lines) with a charging voltage of 280 V leading to a travelled height of 41 cm, b) Corresponding overall peak power of 429.6 kW (3.143.2 kW) with a charging voltage of 280 V.

undercut the targeted height. The explanation for the measured activation energy W being higher than the calculated theoretical value W_1 is, that the primary calculation was made in an ideal state without consideration of any influences of friction and tensions. Another influence on performance is the inertia of the mass to be accelerated.

At the moment of launch, this results in an increased stress level, which then causes a higher actual transformation temperature. This leads to higher temperature values in Equation (4) and thus higher energy needed. To get closer to the targeted flight height, the charging voltage is further increased.

The next set of attempts is made with an increased charging voltage $U_3 = 300$ V, which is just below the technical limits of the voltage supplying transformer. The following discharge of the capacitors via the SMA wires leads to a travel height of the bowling ball of $h_3 = 45$ cm (Figure 11a, dotted red lines), a measured overall system activation energy $W_3 = 495$ J and a combined overall system power $P_3 = 0.49$ MW (Figure 11b).

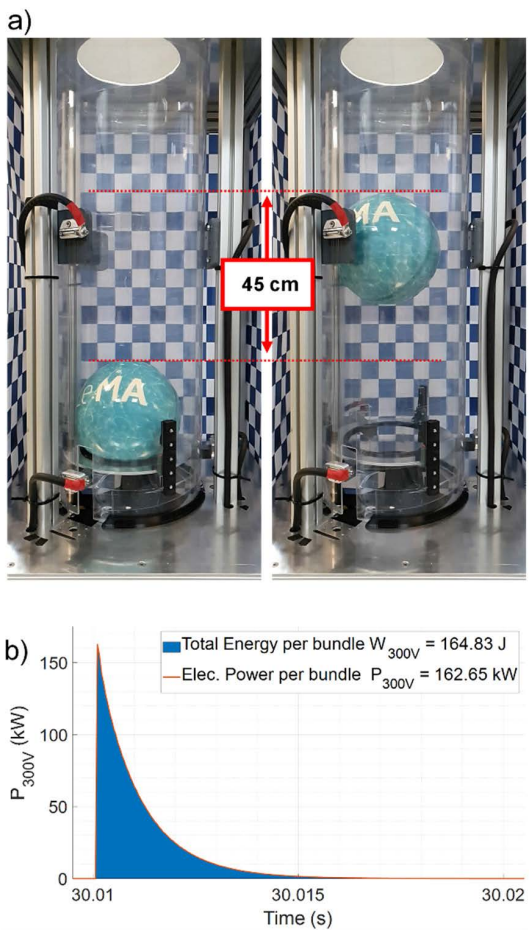

FIGURE 11. a) Comparison of start and end position (red dotted lines) with a charging voltage of 300 V leading to a travelled height of 45 cm, b) Corresponding overall peak power of 488.1 kW (3.162.7 kW) with a charging voltage of 300 V.

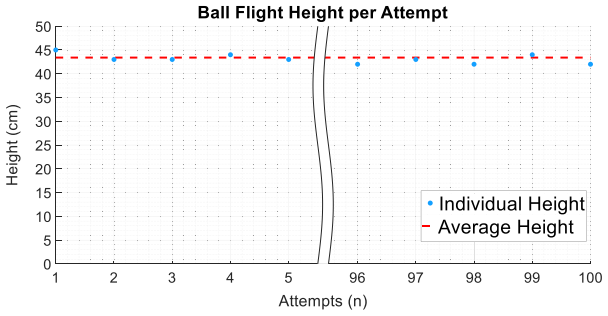

FIGURE 12. Flight heights of the first and last five attempts (solid blue) and the so calculated average flight height (dashed red).

IV. CONCLUSION AND OUTLOOK

In this article, a vivid SMA catapult demonstrator that displays the enormous power potential of SMA technology has been presented. In addition to the development and design of the mechanical structure and actuator components, which successfully launch a bowling ball to the height of about 450 mm, a high-power circuit board is developed, that can deliver a current flow of up to 700 A per board. With a series of fundamental experiments, the reliable functionality and repeatability of the circuit boards is validated. Furthermore, it is shown that the launching sequence can be repeated

without any loss of efficiency being displayed in the constant travelled height of the bowling ball over 100 times (Figure 12). The deviation around the average height value of $h_{avg} = 43.4$ cm can be explained with different ambient temperatures and the resolution of the measuring scale.

The high-speed actuation with the preeminent overall power potential of about 0.5 MW shown by the built demonstrator allows for the option to expand the SMA technology in new areas of application, e.g., load-break switches. The combined high-speed and high-power actuations are a result of the excellent specific energy density of 81.4 kJ/kg and specific power density of 82.2 W/kg of the SMA technology that would hard to be met with competing actuator technologies.

In the next steps, lifetime cycle tests will be conducted in a statistical setup to observe and estimate life cycle times of the used NiTi SMA wires under theses extreme mechanical, thermal and electrical conditions. In addition, the development of a model to predict the behavior of SMA wires in such extreme and highly dynamic conditions will be helpful for the design of commercial applications in the future, as well as further systematic experiments with different loading conditions. Applications that can already be implemented are release mechanisms such as airbag release triggers, load break switches and payload release actuators for space applications.

REFERENCES

[1] R. Pecora and I. Dimino, "SMA for aeronautics," in *Shape Memory Alloy Engineering: For Aerospace, Structural and Biomedical Applications*. Amsterdam, The Netherlands: Elsevier, 2015, pp. 275–304.
[2] M. Kohl, *Shape Memory Microactuators*. Berlin, Germany: Springer, 2004.
[3] T. Duerig, D. Stoeckel, and D. Johnson, "SMA: Smart materials for medical applications," *Proc. SPIE*, vol. 4763, Mar. 2003, Art. no. 508666.
[4] H. Funakubo, *Shape Memory Alloys*, vol. 1. Amsterdam, The Netherlands: Gordon and Breach Science Publication, 1987.
[5] D. Reynaerts and H. Van Brussel, "Design aspects of shape memory actuators," *Mechatronics*, vol. 8, no. 6, pp. 635–656, 1998.
[6] S. J. Furst, "Design, fabrication, and control methods for exploiting the multifunctional sensing and actuation capabilities of shape memory alloy wires," Ph.D. dissertation, Saarland Univ., Saarbrücken, Germany, 2012, doi: 10.22028/D291-22852.
[7] H. Janocha, *Adaptronics and Smart Structures*. Berlin, Germany: Springer-Verlag, 2007.
[8] M. Dolce and D. Cardone, "Mechanical behaviour of shape memory alloys for seismic applications 1. Martensite and austenite NiTi bars subjected to torsion," *Int. J. Mech. Sci.*, vol. 43, no. 11, pp. 2631–2656, 2001.
[9] J. M. Jani, M. Leary, A. Subic, and M. A. Gibson, "A review of shape memory alloy research, applications and opportunities," *Mater. Des.*, vol. 56, pp. 1078–1113, Apr. 2014.
[10] P. Motzki and S. Seelecke, "Industrial applications for shape memory alloys," in *Encyclopedia of Smart Materials*, vol. 4. Amsterdam, The Netherlands: Elsevier, 2022, pp. 254–266.
[11] P. Motzki, F. Khelfa, M. Schmidt, S. Seelecke, and L. Zimmer, "Design and validation of a reconfigurable robotic end-effector based on shape memory alloys," *IEEE/ASME Trans. Mechatronics*, vol. 24, no. 1, pp. 293–303, Feb. 2019, doi: 10.1109/TMECH.2019.2891348.
[12] J. Jeong, K. Hyeon, J. Han, C. H. Park, S.-Y. Ahn, S.-K. Bok, and K.-U. Kyung, "Wrist assisting soft wearable robot with stretchable coolant vessel integrated SMA muscle," *IEEE/ASME Trans. Mechatronics*, vol. 27, no. 2, pp. 1046–1058, Apr. 2022, doi: 10.1109/TMECH.2021.3078472.
[13] W. J. Buehler, J. V. Gilfrich, and R. C. Wiley, "Effect of low-temperature phase changes on the mechanical properties of alloys near composition TiNi," *J. Appl. Phys.*, vol. 34, no. 5, p. 1475, 1963.
[14] F. E. Wang, W. J. Buehler, and S. J. Pickart, "Crystal structure and a unique 'martensitic' transition of TiNi," *J. Appl. Phys.*, vol. 36, no. 10, p. 3232, 1965.
[15] S. Langbein and A. Czechowicz, *Konstruktionspraxis Formgedächtnistechnik*. Bochum, Germany: Springer Vieweg, 2013.
[16] M. Bäker, *Funktionswerkstoffe*. Braunschweig, Germany: Springer Vieweg, 2014.
[17] D. C. Lagoudas, *Shape Memory Alloys*. Boston, MA, USA: Springer, 2008.
[18] H. Jeon, Q. N. Le, S. Jeong, S. Jang, H. Jung, H. Chang, H. J. Pandya, and Y. Kim, "Towards a snake-like flexible robot with variable stiffness using an SMA spring-based friction change mechanism," *IEEE Robot. Autom. Lett.*, vol. 7, no. 3, pp. 6582–6589, Jul. 2022, doi: 10.1109/LRA.2022.3174363.
[19] X.-T. Nguyen, A. A. Calderon, A. Rigo, J. Z. Ge, and N. O. Perez-Arancibia, "SMALLBug: A 30-mg crawling robot driven by a high-frequency flexible SMA microactuator," *IEEE Robot. Autom. Lett.*, vol. 5, no. 4, pp. 6796–6803, Oct. 2020, doi: 10.1109/LRA.2020.3015457.
[20] H. Yang, M. Xu, W. Li, and S. Zhang, "Design and implementation of a soft robotic arm driven by SMA coils," *IEEE Trans. Ind. Electron.*, vol. 66, no. 8, pp. 6108–6116, Aug. 2019, doi: 10.1109/TIE.2018.2872005.
[21] J. Jeong, K. Hyeon, S.-Y. Jang, C. Chung, S. Hussain, S.-Y. Ahn, S.-K. Bok, and K.-U. Kyung, "Soft wearable robot with shape memory alloy (SMA)-based artificial muscle for assisting with elbow flexion and forearm supination/pronation," *IEEE Robot. Autom. Lett.*, vol. 7, no. 3, pp. 6028–6035, Jul. 2022, doi: 10.1109/LRA.2022.3161700.
[22] X. Liu, H. Liu, and J. Tan, "Actuation frequency modeling and prediction for shape memory alloy actuators," *IEEE/ASME Trans. Mechatronics*, vol. 26, no. 3, pp. 1536–1546, Jun. 2021, doi: 10.1109/TMECH.2020.3023097.
[23] H. Jin, Y. Ouyang, H. Chen, J. Kong, W. Li, and S. Zhang, "Modeling and motion control of a soft SMA planar actuator," *IEEE/ASME Trans. Mechatronics*, vol. 27, no. 2, pp. 916–927, Apr. 2022, doi: 10.1109/TMECH.2021.3074971.
[24] P. Motzki, T. Gorges, M. Kappel, M. Schmidt, G. Rizzello, and S. Seelecke, "High-speed and high-efficiency shape memory alloy actuation," *Smart Mater. Struct.*, vol. 27, no. 7, pp. 87–100, 2018.
[25] J. Qiu, J. Tani, D. Osanai, Y. Urushiyama, and D. Lewinnek, "High-speed response of SMA actuators," *Int. J. Appl. Electromagn. Mech.*, vol. 12, nos. 1–2, pp. 87–100, Feb. 2001.
[26] Y. Malka and D. Shilo, "A fast and powerful release mechanism based on pulse heating of shape memory wires," *Smart Mater. Struct.*, vol. 26, no. 9, Sep. 2017, Art. no. 095061.
[27] A. Dana, S. Vollach, and D. Shilo, "Use the force: Review of high-rate actuation of shape memory alloys," *Actuators*, vol. 10, no. 7, p. 140, Jun. 2021.
[28] S. Vollach and D. Shilo, "The mechanical response of shape memory alloys under a rapid heating pulse," *Exp. Mech.*, vol. 50, no. 6, pp. 803–811, Jul. 2010.
[29] V. Brailovski, P. Terriault, T. Georges, and D. Coutu, "SMA actuators for morphing wings," *Phys. Proc.*, vol. 10, pp. 197–203, Jan. 2010.
[30] H. Abuzied, A. Abbas, M. Awad, and H. Senbel, "Usage of shape memory alloy actuators for large force active disassembly applications," *Heliyon*, vol. 6, no. 8, Aug. 2020, Art. no. e04611.
[31] R. Britz and P. Motzki, "Analysis and evaluation of bundled SMA actuator wires," *Sens. Actuators A, Phys.*, vol. 333, Jan. 2022, Art. no. 113233.

PHILIPP MOLITOR received the master's degree in mechatronics and sensor technologies from the Saarland University of Applied Sciences, in 2021. He is currently pursuing the Ph.D. degree in systems engineering with Saarland University, Saarbrücken, Germany. His current research interests include shape memory wires as actuator-sensor systems in high-power applications and elastocaloric cooling systems.

ROUVEN BRITZ received the master's degree in mechatronics from Saarland University, Saarbrücken, Germany, in 2016, where he is currently pursuing the Ph.D. degree in systems engineering. His current research interests include shape memory alloy wires in actuator-sensor systems in industrial and high-power applications.

PAUL MOTZKI received the Ph.D. degree in mechatronics and systems engineering from Saarland University, Saarbrücken, Germany, in 2018. Since 2022, he has been a Professor with the Department of Systems Engineering, Saarland University, in cooperation with the Center for Mechatronics and Automation Technology (ZeMA gGmbH), Saarbrücken, after leading the Research Division "Smart Material Systems," ZeMA, since 2016. His research interests include the development of smart material-based artificial muscles and multifunctional actuator-sensor systems, in particular shape memory alloys, and electroactive polymers.